Targeting mitochondria with small molecules: the preparation of MitoB and MitoP as exomarkers of mitochondrial hydrogen peroxide

Andrew G. Cairns,[†] Stephen J. McQuaker,[†] Michael P. Murphy,[‡] Richard C. Hartley*[†]

[†]WestCHEM School of Chemistry, University of Glasgow, Glasgow, G12 8QQ, UK, E-mail: Richard.Hartley@glasgow.ac.uk
[‡]MRC Mitochondrial Biology Unit, Wellcome Trust/MRC Building, Cambridge, CB2 0XY

Abstract

Small molecules can be physicochemically targeted to mitochondria using the lipophilic alkyltriphenylphosphonium (TPP) group. Once in the mitochondria the TPP-conjugate can detect or influence processes within the mitochondrial matrix directly. Alternatively, the conjugate can behave as a prodrug, which is activated by release from the TPP group either using an internal or external instruction. Small molecules can be designed that can be used in any cell line, tissue or whole organism, allow temporal control, and be applied in a reversible dose-dependent fashion. An example is the detection and quantification of hydrogen peroxide in mitochondria of whole living organisms by MitoB. Hydrogen peroxide produced within the mitochondrial matrix is involved in signalling and implicated in the oxidative damage associated with aging and a wide range of age-associated conditions including cardiovascular disease, neurodegeneration and cancer. MitoB accumulates in mitochondria and is converted into the exomarker, MitoP, by hydrogen peroxide in the mitochondrial matrix. The hydrogen peroxide concentration is determined from the ratio of MitoP to MitoB after a period of incubation, and this ratio is determined by mass spectrometry using d15-MitoP and d15-MitoB as standard.

Here we describe the synthesis of MitoB and MitoP and the deuterated standards necessary for this method of quantification.

1. Introduction

1.1 Mitochondria-targeted drugs and prodrugs

Small molecule drugs are vital to medicine (1). They can often be administered orally, and produce rapid dose-dependent effects. Similarly, small molecules are useful tools to the molecular biologist seeking to elucidate biological processes. A key advantage to small molecules is that in theory they can be used in any cell line, tissue, organ or organism. Their use does not require the manipulation of proteins and gene expression through mutation and RNA-dependent gene silencing, so they can be applied to native tissues and organisms. Furthermore, a small molecule that is useful for the study of a biological process can often be a lead compound for drug discovery, and vice versa.

Mitochondria play a central role in metabolism, supplying most of the ATP used by cells, and also are key to signalling, homeostasis, and the events leading up to apoptosis and necrosis (2,3). Mitochondrial dysfunction contributes to almost every age-associated disease including cardiovascular diseases, neurodegeneration and cancer (2), and is implicated in the process of aging itself (4,5).

Drugs can act on targets in the mitochondria without having an independent mechanism for their accumulation there. However, efficacy would be increased and side-effects decreased if the concentration of a drug is elevated near its site of action. For this reason, it is desirable to have a mechanism of targeting small molecules to the mitochondria, and in particular the mitochondrial matrix where much of

metabolism is sited. Fortunately, there are a variety of approaches for the delivery of molecular cargo to mitochondria (6). These include liposomes (7,8), nanoparticles (9), and peptide sequences (10), but the most general method of delivery involves conjugating the small molecule to a lipophilic delocalized cation (3). The targeting takes advantage of the membrane potential across the mitochondrial inner membrane (MIM).

The electron transport chain (ETC) sited in the MIM pumps protons out of the mitochondrial matrix into the intermembrane space between the MIM and the mitochondrial outer membrane. This gives rise to a small difference in pH and a high membrane potential due to charge separation across the MIM, because the positively charged protons are not accompanied by anions. Thus, the membrane potential ($\Delta\psi$) across the MIM is negative on the matrix side. A proton-motive force resulting from the membrane potential and to a lesser extent the pH gradient drives the production of ATP from ADP and phosphate by ATP-synthase.

Targeting to the mitochondrial matrix can be achieved by incorporating a lipophilic cation in the drug (Figure 2). Lipophilic cations can cross the MIM freely by diffusion both in and out. The positive charge leads to accumulation within the mitochondrial matrix as a result of the membrane potential. The process is governed by the Nernst equation so that for every 60 mV there is a ten-fold accumulation in the matrix relative to the cytosol. This results in a several-hundred-fold higher concentration in the matrix for a membrane potential between 120-180 mV. There is also a small plasma membrane potential that leads to a 3-10 fold accumulation of lipophilic cations within the cell, and this means that the concentration within the mitochondrial matrix may be over a thousand-fold that outside the cell.

It is important to note that the individual lipophilic cations are continually freely diffusing in and out of the mitochondria. If such diffusion is implausible due to size, e.g. some nanoparticles may be too large to cross the MIM (11), then an alternative explanation for accumulation is necessary and the specific localization within the mitochondria needs to be elucidated. Furthermore, the higher concentration within the matrix does not cancel the charge inside; the overall ratio is maintained by the membrane potential and is independent of the concentration of lipophilic cation used, *e.g.* a 300:1 ratio would be maintained if it were 300 nM : 1 nM or if it were 3 μM : 10 nM.

The lipophilic cation of choice is the alkyltriphenylphosphonium (TPP) cation[3] because it has been extensively validated *in vivo*, including in humans, e.g. volunteers in a phase II clinical trial of MitoQ were dosed orally with this mitochondria-targeted antioxidant for 1 year without safety issues (12) (Figure 1). Conjugates of TPP diffuse freely across membranes and the cationic nature of the compounds gives them good water-solubility. TPP is shaped like an inside-out umbrella and so does not intercalate into DNA, which can be a problem for planar lipophilic cations such as phenanthridinium ions (13). The TPP group is small and so it does not adversely affect the physicochemical properties. It is also easily introduced by chemical synthesis (see below).

A wide range of TPP-conjugates have been synthesized and shown to accumulate in mitochondria (Figure 1). Generally, the cargo molecule is not charged, but carboxylic acids that exist predominantly in their anionic carboxylate form at pH7 can be targeted to mitochondria using TPP. Indeed, zwitterionic carboxylate **1** accumulates to a greater extent than the simple triphenylmethylphosphonium cation.

At first sight this may seem perplexing as the zwitterion **1** has no overall charge (Figure 3) (14). The key feature of this system is that the zwitterionic form **1** is too polar to cross membranes but it is in equilibrium with the monocationic carboxylic acid **2**, which is a lipophilic cation and can diffuse freely across the MIM. The carboxylic acid form **2** partitions across the membrane in accordance with the Nernst equation. The carboxylic acid **2** inside the matrix is also in equilibrium with the deprotonated membrane-impermeant zwitterion **1**. If the pH were the same on the inside and outside of the MIM, the zwitterionic form **1** would accumulate to the same degree as the carboxylic acid **2**. However, the pH inside is higher than outside, so accumulation of the zwitterionic form inside is greater than would be expected from the Nernst equation alone.

The TPP-conjugate could be a drug itself, as is the case of MitoQ (15) and most other drug candidates that use the TPP targeting group (Figure 4a). In theory a TPP-drug would distribute throughout the body, concentrating in tissues with high mitochondrial content, such as muscle and liver. However, what if selectivity for a single tissue or site is important? In these cases a prodrug strategy is appropriate whereby the inactive prodrug distributes to all mitochondria, but the drug is released from the TPP targeting group only within particular mitochondria or inside the mitochondria of particular tissues.

Prodrug activation could either be by an instruction from outside the living cells (Figure 4b) or by a process within the mitochondria (Figure 4c), and we have demonstrated both approaches (16,17). MitoPhotoDNP (17) is a UV light-activated mitochondrial uncoupler (Figures 1d and 4b). It accumulates in all mitochondria in accordance with the Nernst equation, but can be activated within particular

mitochondria by irradiation with UV light to release the proton translocator, 2,4-dinitrophenol (DNP). DNP crosses the MIM in both its protonated phenol form and its deprotonated phenoxide form (DNP^-), and so it abolishes the membrane potential of the selected mitochondria, uncoupling the electron-transport chain from ATP-synthase. This gives sustained, but localized disruption of mitochondrial function.

Each cell contains many mitochondria and it is likely that some function well, while others are dysfunctional. The production of reactive oxygen species (ROS) as a result of reduction of oxygen to superoxide by complex I of the ETC in particular, is implicated in the process of ageing and age-related diseases (Figure 5) (18-21). Reverse electron transport through the ETC contributes to the production of superoxide and is greatest when the membrane potential is high (22). Superoxide rapidly disproportionates to hydrogen peroxide and molecular oxygen under catalysis from superoxide dismutase (SOD), and elevated mitochondrial hydrogen peroxide levels appear to contribute to the aged phenotype. Indeed, the free radical theory of ageing suggests that mitochondrial ROS are the main driving force of ageing. It may be tempting to suggest that antioxidants would slow the process of ageing and provide a panacea for the treatment of diseases where damage is mediated or accentuated by oxidative stress. However, this has not proved to be the case (23), possibly because the antioxidants are not distributing to the regions where they are needed. Non-targeted antioxidants may also interfere with intracellular signalling, which is partly mediated by hydrogen peroxide and other ROS.

Targeting antioxidants to the mitochondria ameliorates oxidative damage at the site where most endogenous ROS are generated. Thus, the TPP-antioxidant conjugates MitoQ (15), MitoE (24), and the various TPP-nitroxide conjugates (25-28)

are effective antioxidants that scavenge ROS (Figures 1a and 4a); some of these require in situ reduction to generate the active antioxidant and this provides a route for regeneration. Thus, even though they react stoichiometrically, each molecule can quench many ROS as a result of recycling. MitoQ is an example of this: it is activated as an antioxidant by reduction by the ETC within the mitochondria, is rapidly reactivated after oxidation by ROS (29). Mechanistic mimetics of SOD and peroxidase have also been targeted to mitochondria (Figure 1b) (28,30,31); although these are true catalysts, their turnover rates are significantly slower than endogenous enzymes. On the other hand, the TPP conjugate, MitoSNO (Figure 1c), reduces the production of ROS by inhibiting the mechanism of ROS generation (32). In principle, this is a more efficacious approach because MitoSNO stoichiometrically inhibits the catalytic generation of ROS by the ETC, so that each molecule of MitoSNO prevents the formation of many ROS molecules. MitoSNO limits the damage caused by myocardial infarction *in vivo* by nitrosating Cys39 on the ND3 subunit of complex I of the ETC (33). The nitrosation is reversible, but inhibits the ETC during reperfusion, so minimizing the production of the ROS responsible for reperfusion injury. Importantly, the protein thiol target is only exposed under anoxia: this gives selectivity for affecting dysfunctional mitochondria in the presence of functional mitochondria in other tissues.

MitoSNO acts directly on its target, which is exposed during ischemia. An alternative approach would be to control the release of a drug so that it is only present in dysfunctional mitochondria. Selectivity would then be achieved through activation of a prodrug by processes associated with dysfunctional mitochondria. MitoDNP-SUM is a prototypical example of such a prodrug (Figures 1d and 3c) (17).

ROS are generated when the potential across the MIM is elevated. MitoDNP-SUM accumulates in all mitochondria in accordance with the Nernst equation, and is activated by hydrogen peroxide to release the proton-translocator, DNP. Proton translocation across the MIM is known to reduce the membrane potential. In principle, this provides a negative feedback as mitochondria with lower memberane potentials produce fewer ROS and even a small drop in the membrane potential leads to a large drop in ROS production. The release of DNP from MitoDNP-SUM is mediated by the reaction between the hydroperoxide anion and the arylboronate unit (Figure 6) (17,34). This produces a phenoxide intermediate, which then fragments to release DNP^- and a quinone methide, which rapidly reacts to give a benzylic alcohol side product.

1.2 Mitochondria-targeted sensors

Mitochondrial ROS appear to be important to a wide range of diseases and are central to the free radical theory of aging. Furthermore, there is growing evidence that different ROS have different effects, and that these effects are location and concentration dependent (35). Therefore, a range of mitochondria-targeted sensors have been reported (Figure 7). Nitrone spin traps have been made that react with the highly reactive radicals involved in oxidative stress to give longer lived nitroxyl radicals that can be detected by EPR spectrometry, e.g. MitoPBN (36), MitoSpin (37), MitoBMPO (38) and MitoDEPMPO (Figure 7a) (39,40). Often, the hyperfine couplings allow the type of radical trapped to be identified. The adducts of oxygen-centred radicals are generally short-lived, and superoxide adducts are particularly unstable. However, MitoBMPO and MitoDEPMPO produce distinct,

detectable superoxide adducts (38-40). Unfortunately, high concentrations of the traps are necessary making in vivo work impractical.

An alternative is to detect ROS using fluorescence (41). Superoxide can be detected by Mito-HE (commercially called MitoSOX™ red, Figure 7b) (42), an analogue of hydroethidine targeted to the mitochondria by TPP, gives a specific hydroxylated *N*-alkylphenanthridinium salt, HO-Mito-Etd$^+$, upon reaction with superoxide. The product can be detected using its fluorescence at 579 nm when excited at 510 nm, or by excitation at 396 nm. Exciting at 396 nm minimises confusion arising from other phenanthridinium cations produced by non-specific oxidation. The detection method relies on the fluorescence enhancement that occurs when the phenanthridinium cations intercalates into DNA. Since other phenanthridinium cations also fluoresce, efforts have been made to distinguish and quantify the products of hydroethidine oxidation by HPLC (43). However, the interaction with DNA is problematic as it can hamper extraction of the phenanthridinium cations and could lead to off-target effects resulting in artefacts. Current efforts are focussing on developing synthetic methods (44) to access hydroethidine analogues that are oxidized to hydroxyphenanthridinium cations that do not interact with DNA.

The specific reaction between an arylboronate and hydrogen peroxide or peroxynitrite to give a phenol has been used as an on-switch for a mitochondria-targeted pre-fluorophore, MitoPy1 (Figure 7b) (45,46). The reaction is irreversible, so the rate of increase of fluorescence indicates the concentration of hydrogen peroxide present. Fluorescent probes are easy to use in cell-based studies, but are less useful in whole organisms due to autofluorescence and limited light penetration. One

solution is to express luciferase in an organism and then use a so-called peroxy caged luciferin (e.g. PCL-2) (47,48), which is uncaged by hydrogen peroxide by the mechanism discussed above. The luciferin then undergoes a chemoluminescent reaction catalysed by the expressed luciferase leading to emission of light in response to hydrogen peroxide. However, there is no mitochondria-targeted version of this compound yet.

In summary, the lack of effective methods of detecting specific mitochondrial ROS in vivo had meant that surprisingly little was known about the concentrations of these species in whole living organisms. Indeed, there was no method for the direct determination of how mitochondrial ROS varies with age and with interventions that affect the rate of ageing. This was a serious short-coming as ROS are implicated in almost all the diseases of older age and the free radical theory of aging rests on the proposal that damage from mitochondrial ROS accumulates with age. We recently disclosed that a mitochondria-targeted arylboronate MitoB can be used to determine directly changes in the concentration of mitochondrial hydrogen peroxide in whole organisms (Figure 7c) (49,50). We have reported the use of MitoB in living flies (*Drosophila melanogaster*), nematodes (*Caenorhabditis elegans*), and mice, including providing a detailed step by step protocol (33,49,50), and are now investigating its application to fish. Since these reports include detailed descriptions of how MitoB is employed, we will only provide a very brief overview of the main features of this probe. On the other hand, we report here a detailed protocol for the synthesis and purification of MitoB and all the chemical standards needed for its use.

MitoB has a TPP group that causes it to accumulate in mitochondria. Following injection into the organism, MitoB rapidly distributes to the various

tissues of the body so that about 90% of the probe is intracellular and 98% of this is within the mitochondria. It reacts with hydrogen peroxide to give the phenol, MitoP (Figure 8). More precisely, it reacts with the conjugate base of hydrogen peroxide, the hydroperoxide anion, so that the higher pH of the mitochondrial matrix gives an additional four-fold acceleration relative to reaction in the cytosol. With the exception of peroxynitrite and HOCl, other ROS do not react with MitoB to give this product (51,52). Importantly, the rate constant for reaction between the mitochondrial peroxidase, peroxiredoxin III, and hydrogen peroxide is over a million times higher than that for reaction with MitoB (49). Since MitoB reacts slowly, it does not itself influence the hydrogen peroxide concentration.

Both MitoB and MitoP can be easily detected by electrospray ionization mass spectrometry (ESI-MS) with high sensitivity, because each molecule already bears a fixed positive charge and does not need to be ionized to be detected. As MitoB is converted irreversibly into MitoP, the ratio of MitoP to MitoB increases with time. The rate of this increase reflects the concentration of hydrogen peroxide. The concentration of MitoB in the mitochondrial matrix is about 3000 times the extracellular concentration, and this combined with higher proportion of hydrogen peroxide in its deprotonated form means that MitoP production occurs almost exclusively in the mitochondrial matrix. Expressing the amount of MitoP and MitoB as a ratio corrects for absolute concentration.

To date, we have determined the ratio of MitoP to MitoB following euthanasing the animals, but in principle the ratio of MitoP to MitoB in fluids such as blood or urine might be used to monitor hydrogen peroxide concentrations continuously because both MitoP and MitoB freely diffuse in and out of

mitochondria. However, in all cases quantification requires correction for extraction efficiency. This is done by adding a known quantity of d15-MitoB and deuterated d15-MitoP after the experiment is complete and before extraction of the MitoB and MitoP. For convenience both deutero standards are prepared from perdeutero triphenylphosphine so there are 15 labels in each. Thus, the amount of MitoP (*m*/*z* 369) is determined by comparison with d15-MitoP (*m*/*z* 384), and the amount of MitoB (*m*/*z* 397) is determined relative to d15-MitoB (*m*/*z* 412). Liquid chromatography (LC) is used to separate the TPP compounds from other endogenous compounds extracted with them. Often the TPP compounds elute at the same time, and the compounds are detected simultaneously using multiple reaction monitoring [for details of this and the comparison with the deutero standards see Cochemé *et al.* (49,50)]. Depending on the LC system used, there may be some or complete separation of MitoB from MitoP, and indeed partial separation of the deutero labelled and unlabelled version of the compounds is also possible (53-55). Therefore, it is important to sample the ions over the whole peak so that the proportions are correct.

MitoP is an exomarker (56) of mitochondrial hydrogen peroxide in living organisms (Figure 9). This is similar to a biomarker, but is produced by a specific transformation of an exogenous probe, in this case MitoB. Whereas biomarkers may be produced by a range of processes, a small molecule probe can be designed to detect a specific endogenous compound, in this case hydrogen peroxide, in a particular place, e.g. the mitochondria. Exomarkers have the advantage that they are neither produced nor degraded by endogenous processes and so reflect more accurately the concentration of the species they are designed to detect. An

exomarker approach to the detection of mitochondrial glyoxal and methylglyoxal has also been developed using MitoG (Figure 7c) (57).

Detailed protocols for the preparation of MitoB, d15-MitoB, MitoP and d15-MitoP are provided below.

2. Materials

2.1 Equipment for Synthesis

1. UV lamp (to check TLC plates, 254 nm)
2. Oven (200 °C+ capable)
3. Fridge (0 - 5 °C capable)
4. Stirring/heating plate with temperature probe
5. Oil bath or alternative heating media
6. Rotary evaporator (in fume hood) attached to vacuum line
7. Vacuum pump (weak vacuum, 100 mbar sufficient)
8. Vacuum line (<20 mbar)
9. Inert gas supply (approximately atmospheric pressure, balloon sufficient), attached to a short needle
10. Dewar-type bowl (large enough for the 50 mL flask and coolant)
11. Thermometer (effective down to at least −20 °C)
12. Desiccator
13. 1 x clamp stand and appropriate clamps
14. 2 x 50 mL round bottomed flask

15. 3 x 100 mL round bottomed flask
16. 2 x 250 mL round bottomed flask
17. 1 x condenser (appropriate to fit flask) and connections to attach water
18. 5 x suba seals to fit condenser and flasks
19. 2 x Magnetic stirrer bar
20. 100 or greater mL Buchner flask and small buchner funnel with filter paper or equivalent filtration set up
21. 1 L or greater mL Buchner flask and large (500 mL) buchner funnel with filter paper or equivalent filtration set up
22. 50 mL beaker
23. 2 x 1 L beaker or conical flask
24. Appropriate sample vials (10 mL)
25. Glass pipettes and pipette teats
26. 1 mL syringes and appropriate needles
27. 2 x 20 mL syringe
28. 1 x 50 mL syringe
29. 4 x long metal needle
30. Chromatography grade silica gel (SiO_2) and acidified sand
31. 2 x TLC plates and appropriate tank
32. NMR tube and access to NMR machine

2.2 Synthesis of MitoB

1. Toluene (irritant, health hazard, flammable)
2. Triphenylphosphine (harmful, health hazard)

3. (3-bromomethyl)phenylboronic acid (irritant)
4. dimethyl sulfoxide (irritant)
5. Distilled water
6. Diethyl ether (flammable, harmful)
7. d_6-dimethyl sulfoxide (irritant)

2.3 Synthesis of d15-MitoB

The same materials as for MitoB, except replace triphenylphosphine with d15-triphenylphosphine.

2.4 Synthesis of MitoP

1. 3-hydroxymethylbenzylalcohol (harmful/irritant, corrosive)
2. Phosphorus tribromide (1 M solution in dichloromethane, corrosive, harmful/irritant)
3. Anhydrous pyridine (harmful/irritant, flammable)
4. Anhydrous acetonitrile (harmful/irritant, flammable)
5. Anhydrous toluene (irritant, health hazard, flammable)
6. Triphenylphosphine (harmful, health hazard)
7. Ethyl acetate (irritant, flammable)
8. Diethyl ether (harmful, flammable)
9. Dichloromethane (harmful, health hazard)
10. Ethanol (flammable)
11. Distilled water
12. Dry ice ($CO_{2(s)}$, may cause burns, $CO_{2(g)}$ hazardous above 1.5% concentration)

13. Acetone or 2-isopropanol (flammable, irritant)
14. d_6-dimethyl sulfoxide
15. Magnesium Sulfate

2.5 Synthesis of d15-MitoP

The same materials as for MitoP, except replace triphenylphosphine with d15-triphenylphosphine.

3. Method

3.1 Overview of procedure for the synthesis of MitoB and d15-MitoB

MitoB was prepared from commercially available 3-(bromomethyl)phenylboronic acid using triphenylphosphine to displace the benzylic bromide (Figure 10). The procedure produces the bromide salt (MW 477.14). The reaction is carried out in boiling toluene under reflux and the MitoB bromide precipitates from solution. The solid MitoB bromide is collected by filtration and then recrystallized from DMSO. MitoB is an arylboronic acid and can dehydrate to form a trimer, so a final recrystallization from water is carried out to ensure MitoB bromide is entirely in the boronic acid form. d15-MitoB bromide is prepared in exactly the same way except d15-triphenylphosphine is used instead of triphenylphosphine.

3.2 Setup for preparation of MitoB and d15-MitoB (*see* **Note 1**)

1. For the preparation of MitoB, weigh out 1.00 g (4.65 mmol, 1.00 eq.) 3-(bromomethyl)phenylboronic acid and 1.34 g (5.11 mmol, 1.10 eq.) triphenylphosphine and add both to the 50 mL round bottomed flask containing the magnetic stirrer bar (*see* **Note 2**). Alternatively, for the preparation of d15-MitoB, weigh out 1.00 g 3-(bromomethyl)phenylboronic acid and 1.42 g d15-triphenylphosphine and add both to the 50 mL round bottomed flask.
2. Clamp the flask around the ground glass joint to the clamp stand, arranged so it is centrally positioned in the heating medium on top of the stirrer plate. Add 25 mL toluene.
3. Attach the condenser to the flask, adding a suba seal and inert gas inlet to the top of the condenser by way of a needle piercing the suba seal. Attach water supply to the condenser.
4. Insert a second needle in the suba seal to act as an outlet and purge the flask and condenser with the inert gas for 5 min.
5. Start the stirring and then set the reaction to heat to reflux. The boiling point of toluene is 110-111 °C.
6. When the boiling temperature is reached, continue to heat the reaction under reflux for 6 h for complete conversion to product, which precipitates as a solid (*see* **Note 2**).
7. Turn off heat and remove the reaction from the heat source by moving clamp arm bearing the flask upward. Allow to cool for 30 min. Meanwhile heat 20 mL toluene to 70 °C in the 100 mL round bottomed flask.

8. Filter under vacuum to collect the solid MitoB bromide. Re-use the filtrate to wash out the contents of the round bottomed flask pouring the washings over the filter cake of MitoB bromide. Wash out the flask twice with the hot toluene (10 mL each wash, preheated to 70 °C) again pouring the washings over the filter cake of MitoB bromide. Finally wash the filter cake followed with 30 mL diethyl ether. Allow the material to further dry under vacuum for 20 min.

3.3 Purification of MitoB

1. Add approximately 500 mg of solid crude MitoB bromide to 0.7 mL of dimethyl sulfoxide and heat to dissolve in a sample vial. Allow the material to cool, crystallize and settle (1 h) (*see* **Note 3**).
2. Carefully remove the dimethyl sulfoxide with a pipette (leave the crystals behind).
3. Repeat steps 1 and 2 with more solid crude MitoB bromide, reusing the dimethyl sulfoxide from the previous crystallisation (*see* **Note 4**) and an additional 0.1 mL (measured with a 1 mL syringe and used to wash the residual material through the empty pipette following transfer) until all crude material has been recrystallized (you will now have up to five vials each containing approximately 400 mg recrystallized material).
4. After removing the dimethyl sulfoxide from each sample vial, add 1.5 mL of hot distilled water, agitate and allow to settle before carefully removing the liquid with a pipette, leaving the solid MitoB bromide in the vial. Combine these waste aqueous solutions and the final waste dimethyl sulfoxide, then

collect any further crystals formed, retrieving the final batch of crystals by vacuum filtration if necessary, re-using the previously mentioned apparatus.

5. Combine the batches of crystallized MitoB bromide in a 100 or greater mL round bottomed flask, using hot distilled water in 1 mL aliquots to wash any residual solid into the flask.
6. Add distilled water to a volume of 40-50 mL and heat to 80 °C on the rotary evaporator at ambient pressure for 1 h, then allow the heating bath to cool to 50 °C and carefully concentrate the water under vacuum until a white solid is observed forming on the flask walls (*see* **Note 5**).
7. When solid is observed, remove the flask and allow it to cool. The MitoB bromide continues to precipitate from solution. Collect the solid by filtering under vacuum as previously, allowing 30 min-1 h (depending on vacuum strength) to dry the solid material. The filtrate can be reused to obtain more MitoB bromide if desired, by further concentrating as in step 5.
8. Collect the material in a pre-weighed vial and check purity (if possible) by ^{1}H NMR in *d*$_6$-dimethyl sulfoxide, with approx. 2 mg of material in a 0.5 mL sample (s*ee* **Note 6**).

Approximate Yield: 70%

3.4 Characterization data for MitoB

δ_H (500 MHz, *d*$_6$–dimethyl sulfoxide): 7.95 [2H, s, B(O**H**)$_2$], 7.92-7.86 (3H, m, 3 x *p*-PPh$_3$), 7.77-7.68 (7H, m, 6 x *o*-PPh$_3$, H4), 7.67-7.58 (6H, 6 x *m*-PPh$_3$), 7.46 (1H, s, H2), 7.18 (1H, t, *J* = 7.6 Hz, H5), 6.94 (1H, d, *J* = 7.6 Hz, H6), 5.11 (2H, *J* = 15.6 Hz, C**H**$_2$Ph).

δ_C (100 MHz, *d*$_6$–dimethyl sulfoxide): 136.88 (d, J = 5.6 Hz, CH), 134.94 (d, J = 2.4 Hz, CH), 133.93 (d, J = 9.8 Hz, CH), 133.78 (d, J = 3.6 Hz, CH), 132.25 (d, J = 5.2 Hz, CH), 129.95 (d, J = 12.5 Hz, CH), 127.60 (d, J = 2.8 Hz, CH), 126.67 (d, J = 8.5 Hz, C), 117.75 (d, J = 85.5 Hz, C), 28.15 (d, J = 46.5 Hz, CH_2).

δ_P (162 MHz, *d*$_6$–dimethyl sulfoxide) 23.15 (s).

IR (ATR, cm^{-1}): 3322 (OH), 2928 (ArH, v. weak), 2882 (ArH), 2789 (ArH, v. weak), 1549 (Ar, v. weak), 1485 (Ar, weak), 1435 (Ar, strong). LRMS (ESI): 397 [M+ (phosphonium cation), 100%].

HRMS: 397.1518 [M+ (phosphonium cation)]. $C_{25}H_{23}{}^{11}BO_2P$ requires 397.1524.

Microanalysis: $C_{25}H_{23}BBrO_2P$ requires C: 62.93% H: 4.86%, found C: 62.90% H: 4.80%.

3.5 Characterization data for d_{15}-MitoB:

δ_H (400 MHz, *d*$_6$–dimethyl sulfoxide): 92:8 mixture of d_{15}:d_{14}: 7.97 [2H, s, B(O**H**)$_2$], 7.74-7.69 (1H, m, H4), 7.46 (1H, s, H2), 7.17 (1H, t, *J* = 7.6 Hz, H5), 6.94 (1H, d, *J* = 7.6 Hz, H6), 5.12 (2H, *J* = 15.6 Hz, C**H**$_2$Ph). δ_C (100 MHz, *d*$_6$–dimethyl sulfoxide): 137.02 (d, J = 5.6 Hz, CH), 135.08-134.22 (m, CD), 133.92 (d, J = 2.7 Hz, CH), 134.22-133.12 (m, CD), 132.43 (d, J = 5.5 Hz, CH), 130.05-129.15 (m, CD), 127.75 (d, J = 2.6 Hz, CH), 126.84 (d, J = 8.6 Hz, C), 117.67 (d, J = 85.4 Hz, C), 28.27 (d, J = 46.5 Hz, CH2). δP (162 MHz, *d*$_6$–dimethyl sulfoxide): 23.01 (s). IR (ATR, cm^{-1}): 3236 (OH), 2928 (ArH, v. weak), 2882 (ArH), 1543 (Ar), 1485 (Ar), 1424 (Ar, moderately strong). LRMS (ESI): 412 [M+(phosphoniumcation), 100%]. HRMS: 412.2460 [M+(phosphonium cation)]. $C_{25}H_{23}{}^{11}BO_2P$ requires 412.2465. Microanalysis: $C_{25}H_8D_{15}BBrO_2P$ requires C: 61.00% H: 1.64% D: 6.14%, found C: 60.90% H: 1.64% D: 6.17%.

d_{14} peaks observed: δ_H (400 MHz, d_6–dimethyl sulfoxide): 7.89 (0.02H, d, J = 2.0 Hz, *p*-PPh_3), 7.63 (0.03H, d, J = 12.7 Hz, *o*-PPh_3), 7.24 (0.03H, d, J = 8.0 Hz, *m*-PPh_3).

3.6 Overview of procedure for the synthesis of MitoP and d15-MitoP (*see* Note 7)

MitoP is prepared in two steps by an adaptation of the procedure described by Dawson *et al.* (58) (Figure 11). First, in reaction A, 3-hydroxybenzyl alcohol is converted into the 3-(bromomethyl)phenol by reaction with phosphorus tribromide in a mixture of anhydrous pyridine and anhydrous acetonitrile. The reaction is water-sensitive and phosphorus tribromide reacts violently with water. 3-(Bromomethyl)phenol is a reactive compound and should be used for the next step soon after preparation. The second step, reaction B, involves displacing the benzylic bromide with triphenylphosphine to give MitoP bromide. The reaction is carried out in boiling toluene under reflux and MitoP bromide precipitates from solution. Often the MitoP is essentially pure after work-up, but recrystallization from ethanol is possible if impure material is obtained. d15-MitoP bromide is prepared by using d15-triphenylphosphine instead of triphenylphosphine in reaction B.

3.7 Setting up reaction A

1. Dry one 50 mL and two 100 mL round bottomed flasks and appropriate stirrer bars, the metal needles and the condenser overnight in a dry 250 °C oven. Alternatively, the flasks can be dried under vacuum with a heat gun or Bunsen burner (do not do this with the condenser). The dry glassware, needles and stirrer bars should be allowed to cool under vacuum and kept in a sealed dessicator prior to use.

2. Prepare a -15 °C bath on a stirrer plate by adding dry ice to 2-isopropanol or acetone in a dewar, checking with a thermometer. Err on the cold side: somewhat below -15 °C is acceptable, but above this temperature is not satisfactory. (*see* **Note 8**).
3. Attach anhydrous acetonitrile, phosphorus tribromide solution and anhydrous pyridine to an inert gas supply.
4. Set up the 50 mL flask in the dewar, sealing with a suba seal and connecting to inert gas.

3.8 Reaction A

1. Add 14.1 mL phosphorus tribromide solution and 5 mL acetonitrile to a 100 mL round bottomed flask using long needles attached to syringes, then stir the mixture. Immediately return the acetonitrile needle and syringe to a dry, inert environment for later use (putting the needle back through a seal into the dry solvent container with the syringe still attached is sufficient). Quench the phosphorus tribromide needle into 20 mL dichloromethane then add 5 mL ethanol to this solution. Dispose of this as toxic waste.
2. Add 0.75 mL anhydrous pyridine dropwise over 10 min with a needle and syringe to the stirring mixture (*see* **Note 9**).
3. Dissolve 5 g 3-hydroxymethylbenzyl alcohol in 15 mL anhydrous acetonitrile and 0.25 mL anhydrous pyridine in a 50 mL round bottomed flask (*see* **Note** 10), then add the solution to the reaction mixture dropwise over 10 min using a long needle and 20 mL syringe. An additional 2 mL anhydrous acetonitrile

can then be used to wash any residual material from the 50 mL round bottomed flask into the reaction mixture.

4. Allow the reaction to stir and warm gradually to room temperature over 4 h.

3.9 Workup of Reaction A (*see* **Note 11**)

1. Prepare 2 L 19:1 dichloromethane/ethyl acetate.
2. Use 300 mL of this solution to make a slurry with approximately 250 mL SiO_2 in a 1 L beaker or conical flask, then load this into the large Buchner funnel. Allow the solvent to run through to incipient wetness, agitating gently to aid silica settling, then top with a 1 cm layer of acidified sand.
3. Transfer the reaction mixture from reaction A to a 250 mL round bottomed flask, washing the residue in with dichloromethane (*see* **Note 12**), then remove the solvent under reduced pressure in a fume hood, disposing of the distillate as toxic waste.
4. Dissolve the residue in 100 mL dichloromethane, then wash with 100 mL H_2O, re-extracting with a further 100 mL dichloromethane (*see* **Note 11**).
5. Add the combined dichloromethane solutions to the silica in the Buchner funnel, allowing the solvent to run through under atmospheric pressure until no residual solvent remains above the silica layer, discarding the resulting filtrate. Add 1 cm sand and elute the compound under vacuum with the dichloromethane/ethyl acetate solution, collecting fractions of approximately 300 mL (*see* **Note 13**), then spotting each on a silica TLC plate in turn and stopping when the last fraction shows no UV activity under an appropriate lamp. Confirm the product fractions by TLC (R_f = 0.57 in 9:1

dichloromethane/ethyl acetate) and combine these in a 1 L beaker or conical flask.

6. Add magnesium sulfate to the filtrate and swirl, then filter the solution, using dichloromethane to wash any residual material from the magnesium sulfate.
7. Half fill a 250 mL round bottomed flask with a portion of the solution, and remove the solvent under reduced pressure, add a further portion of the solution and repeat until all the material is contained in the flask and all solvent has been removed.

3.10 Characterization data for 3-(bromomethyl)phenol:

δ_H (500 MHz, $CDCl_3$): 7.21 (1H, t, *J* = 7.9 Hz, H5) 6.97 (1H, d, broad, *J* = 7.7 Hz, H4), 6.88 (1H, t, *J* = 2.1 Hz, H2), 6.77 (1H, ddd, *J* = 8.1, 2.5, 0.7 Hz, H6), 4.44 (2H, s, CH_2). δ_C (100 MHz, $CDCl_3$): 155.75 (C), 139.56 (C), 120.20 (CH), 121.63 (CH), 116.07 (CH), 115.69 (CH), 33.27 (CH_2). IR (ATR cm^{-1}): 3354 (O-H), 1591 (C_{Ar}=C_{Ar}), 1489 (C_{Ar}=C_{Ar}), 1456 (C_{Ar}=C_{Ar}). LRMS (EI^+): 187.99 ($^{81}BrM^{+\cdot}$, 31%), 185.99 ($^{81}BrM^{+\cdot}$, 33%), 107.06 [(M^+ − Br), 100%]. HRMS: 187.9652 and 185.9686. C_7H_7OBr requires 187.9660 and 185.9680. MP: 60 - 63 °C.

3.11 Setting up reaction B

1. Add 70 mL dry toluene, a suitable stirrer bar and 10 g triphenylphosphine to the reaction A product.
2. Attach the condenser to the water and round bottomed flask; put under inert gas and heat to reflux while stirring for 6 h.

3.12 Work up of reaction B

1. Warm 100 mL toluene to 70 °C in a 250 mL round bottomed flask.
2. Filter the reaction mixture vacuum, re-using the filtrate to wash out the contents of the flask, then wash out the flask with a further 2 x 50 mL 70 °C toluene and use these to further wash the filter cake, followed by 100 mL diethyl ether. Allow the material to further dry under vacuum for 20 min.
3. Check purity by ^{1}H NMR in d_6-dimethyl sulfoxide. Proceed to Section 3.13 only if necessary

Approximate Yield (2 steps): 75%

3.13 Purification (if necessary)

1. Add ethanol to the impure solid in a ratio of 15 mL/g in a large round bottomed flask (100 mL for 1 g, *see* **Note 14**) then heat the mixture to 80 °C until the solid dissolves.
2. Remove the flask from the heat, allow to cool and seal with a suba seal (*see* **Note 15**), then place in a fridge (approx. 5 °C) for 5-6 hours (*see* **Note 16**).
3. Decant the solvent from the crystals, then re-dissolve the crystals in a minimal quantity of warm ethanol and add distilled water to reach an approximate ratio of 2:1 ethanol/water.
4. Carefully remove the solvent mixture under reduced pressure to retrieve the pure solid (*see* **Note 17**).

3.14 Characterization data for MitoP bromide

δ_H (400 MHz, d_6–dimethyl sulfoxide): 9.54 (1H, s, OH), 7.94-7.86 (3H, m, 3 × *p*-H PPh_3), 7.78-7.70 (6H, m, 6 × *m*-H PPh_3), 7.70-7.60 (6H, m, 6 × *o*-H PPh_3), 7.00 (1H, t, *J* = 7.8 Hz, H-5), 6.68 (1H, broad d, *J* = 8.0 Hz, H-6), 6.41 (1H, broad s, H-2), 6.36 (1H, broad d, *J* = 7.1 Hz H-4), 5.06 (2H, d, *J* = 15.6 Hz, CH_2). δ_C (100 MHz, d_6–dimethyl sulfoxide): 157.54 (d, *J* = 3.2 Hz, C), 135.10 (d, *J* = 1.9 Hz, CH), 134.03 (d, *J* = 9.8 Hz, CH), 130.11 (d, *J* = 12.5 Hz, CH), 129.75 (d, *J* = 2.2 Hz, CH), 129.05 (d, *J* = 8.3 Hz, C),121.39 (d, *J* = 5.5 Hz, CH), 117.98 (d, *J* = 85.6 Hz, C), 117.83 (d, *J* = 5.6 Hz, CH), 115.33 (d, *J* = 3.1 Hz, CH), 28.13 (d, *J* = 46.6 Hz, CH_2). δ_P (162 MHz, d_6–dimethyl sulfoxide): 23.03(s). IR (ATR, cm^{-1}): 3079 (OH), 2889 (ArH), 2858 (ArH), 2787 (ArH), 1611 (Ar), 1568(Ar). LRMS (ESI): 369 [M+(phosphonium cation), 100%]. HRMS:369.1399 [M+(phosphonium cation)]. $C_{25}H_{22}OP$ requires 369.1403. Microanalysis: $C_{25}H_{22}BrOP$ requires C: 66.83% H: 4.94%, found C: 66.89% H: 4.98%.

3.15 Characterization data for d_{15}-MitoP bromide

δ_H (400 MHz, d_6–dimethyl sulfoxide): 9.55 (1H, s, OH), 7.00 (1H, t, *J* = 7.8 Hz, H-5), 6.69 (1H, broad d, *J* = 8.0Hz, H-6), 6.42 (1H, broad s, H-2), 6.36 (1H, broad d, *J* = 7.2 Hz, H-4), 5.08 (2H, d, *J* =15.7 Hz, CH_2). δ_C (100 MHz, d_6–dimethyl sulfoxide): 157.54 (d, *J* = 3.1 Hz, C), 134.90-134.23 (m, CD), 134.08- 133.12 (m, CD), 130.08-129.20 (m, CD), 129.73 (d, *J* = 3.4 Hz, CH),128.57 (d, *J* = 8.6 Hz, C), 121.39 (d, *J* = 5.6 Hz, CH), 117.85 (d, *J* = 5.5 Hz, CH), 117.76 (d, *J* = 85.4 Hz, C), 115.32 (d, *J* = 3.4 Hz, CH), 28.16 (d, *J* = 46.6 Hz, CH_2). δ_P (162 MHz, d_6–dimethyl sulfoxide): 22.92 (s). IR (ATR, cm–1): 3080 (OH), 2889 (ArH), 2858 (ArH), 2787 (ArH), 1617 (Ar), 1609 (Ar), 1587 (Ar). LRMS (ESI): 384 [M+(phosphonium cation),100%]. HRMS: 384.2336 [M+

(phosphonium cation)]. $C_{25}H_7D_{15}OP$ requires 384.2344. Microanalysis: $C_{25}H_7D_{15}BrOP$ requires C: 64.66% H: 1.52% D: 6.51%, found C: 64.69% H: 1.52% D: 6.69%.

4. Notes

1. Although reasonably dry conditions and toluene are preferable, use of all reagents including toluene as supplied commercially produces acceptable results for this synthesis.

2. Where more than one size is suitable for step 4, (Section 3.2) a larger stirrer bar is preferred, as substantial precipitate is generated and may impede a smaller one.

3. The synthesis as outlined does not require a centrifuge for Section 3.3 step 1, and the yield given can be achieved without one. However, where available use of a centrifuge to settle the fine precipitate from the crystallisations will make the purification considerably easier.

4. Re-use of the recrystallization liquors (Section 3.3, steps 1-3) is important as excess dimethyl sulfoxide is relatively difficult to remove, and MitoB is fairly soluble in this solvent - the first 500 mg batch will saturate the solvent. Recrystallisation of all the material in a larger quantity of dimethyl sulfoxide works but has a detrimental impact on yield.

5. Protodeboronation is possible in step 6 (Section 3.3); increasing the temperature of the aqueous crystallization beyond 80 °C appears to accelerate this reaction. If this product is observed, repeating step 6 (Section 3.3) and concentrating the sample less may be sufficient to remove this; otherwise repeat Section 3.3. ^{1}H NMR of impurity: δ_H (400 MHz, d_6–dimethyl sulfoxide): 7.95-7.87 (3H, m, 3 x *p*-PPh$_3$), 7.79-7.70 (6H, m, 6 x *o*-PPh$_3$), 7.69-7.61 (6H, 6 x *m*-PPh$_3$), 7.34-7.27 (1H, m, H4), 7.23 (2H, t, J = 7.7 Hz, H2, H6), 6.99-6.93 (2H, m, H3, H5), 5.14 (2H, d, J = 15.8 Hz, C**H**$_2$Ph).

6. The concentration of the ^{1}H NMR sample for Section 3.3 step 8 is not experimentally vital, but is specified as much stronger samples will show a second set of peaks if the d_6-dimethyl sulfoxide is dry; these represent trimerisation of the boronic acid within the NMR sample rather than degradation of the material. If side peaks are observed, add a drop of water to the NMR to check trimerisation is not responsible.

7. If possible higher purity 3-hydroxymethylbenzyl alcohol (95%) should be used, as this allows the compound to be isolated in sufficient purity to avoid recrystallization (Section 3.6).

8. Care should be taken in preparation of cold bath (Section 3.7, Step 2) not to add a large excess of dry ice, as temperatures significantly below the freezing point of acetonitrile can be achieved with such conditions.

9. Addition of the pyridine will produce white gas. Addition of a vent will dissipate this, however positive argon pressure should be maintained while the vent is in place (Section 3.8, Step 1).

10. Dissolution of the starting material is slow in Section 3.8, Step 3. Sonication significantly speeds up this process.

11. Section 3.9, and particularly Step 4, should be performed quickly - the product is not stable indefinitely and will react with water present to reform starting material. Even the crystalline solid isolated (Step 7) may decompose relatively quickly if not used, especially if heated or impure. For this reason it is not desirable to heat this compound strongly to remove solvent traces. These will not interfere with the following reaction anyway, but may instead be removed under higher vacuum if desired.

12. During Step 3 (Section 3.9) a significant portion of the material will appear to be insoluble, however the desired product will dissolve in dichloromethane.

13. Only a small number of fractions (5 or less) are expected for Step 5 (Section 3.9). Do not increase the solvent polarity as side products or starting material may elute.

14. The procedure outlined for recrystallization (Section 3.13) uses enough ethanol to fully dissolve 1 g of Mito P. This will often be unnecessary where

purity is high (90%+) already. Less ethanol can be used; it is not necessary to fully dissolve the material prior to cooling in these cases.

15. Reasonable substitutes may be used for the suba seal (Section 3.13, Step 2); be aware however that warm ethanol vapour will start to dissolve parafilm and that the drop in temperature on cooling will result in a vacuum and make glass stoppers difficult to remove.

16. In our experience 80%+ of the Mito P will crystallize out in the time given (Section 3.13, Step 2), but it is likely that leaving the crystallisation longer would increase the yield slightly.

17. Evaporation in ethanol/water mix is to remove residual ethanol (Section 3.13, Step 4). Care is required as 'bumping' is likely towards the end of this evaporation (the use of the larger flask size somewhat mitigates this problem). In our experience traces of ethanol are difficult to remove from solid even with prolonged heating under vacuum.

Acknowledgements

AC funded through a European Research Council Advanced Grant (322784) to Neil Metcalfe, SJMcQ through Lloyds TSB Foundation for Scotland and the Royal Society of Edinburgh. We thank the EPSRC National Mass Spectrometry Service at Swansea University for ESI-MS, both LRMS and HRMS.

References

1. Nielsen T.E., Schreiber S.L. (2008) Diversity-oriented synthesis - Towards the optimal screening collection: A synthesis strategy. *Angew Chem Int Ed* **47**, 48-56.

2. Smith R.A.J., Hartley R.C., Cochemé H.M., Murphy M.P. (2012) Mitochondrial pharmacology. *Trends Pharmacol Sci* **33**, 341-352.

3. Smith R.A.J., Hartley R.C., Murphy, M.P. (2011) Mitochondria-Targeted Small Molecule Therapeutics and Probes. *Antioxid Redox Signal* **15**, 3021-3038.

4. Logan A., Shabalina I.G., Prime, T.A. et al. (2014) In vivo levels of mitochondrial hydrogen peroxide increase with age in mtDNA mutator mice. *Ageing Cell* **13**, in press.

5. Lepez-Otin C., Blasco M.A. Partridge, L. et al. (2013) The Hallmarks of Aging. *Cell* **153**, 1194-1217.

6. Jean S.R., Tulumello D.V., Wisnovsky S.P. et al. (2014) Molecular Vehicles for Mitochondria! Chemical Biology and Drug Delivery. *ACS Chem Biol* **9**, 323-333.

7. Weissig V., Boddapati S.V., Cheng S.M. et al. (2006) Liposomes and liposome-like vesicles for drug and DNA delivery to mitochondria. *J. Liposome Res* **16**, 249-264.

8. Boddapati S.V., D'Souza G.G.M., Erdogan S. et al. (2008) Organelle-targeted nanocarriers: Specific delivery of liposomal ceramide to mitochondria enhances its cytotoxicity in vitro and in vivo. *Nano Lett* **8**, 2559-2563.

9. Marrache S., Dhar S. (2012) Engineering of blended nanoparticle platform for delivery of mitochondria-acting therapeutics. *Proc Natl Acad Sci USA* **109**, 16288-16293.

10. Stewart K.M., Horton K.L., Kelley S.O. (2008) Cell-penetrating peptides as delivery vehicles for biology and medicine. *Org Biomol Chem* **6**, 2242-2255.

11. Horobin R.W. (2010) Can QSAR Models Describing Small-Molecule Xenobiotics Give Useful Tips for Predicting Uptake and Localization of Nanoparticles in Living Cells? And If Not, Why Not?, In Weissig V., D'Souza G.G. (eds) Organelle-Specific Pharmaceutical Nanotechnology. Wiley, NY.

12. Snow B.J., Rolfe FL, Lockhart MM et al. A Double-Blind, Placebo-Controlled Study to Assess the Mitochondria-Targeted Antioxidant MitoQ as a Disease-Modifying Therapy in Parkinson's Disease. *Movement Disord.* **25**, 1670-1674 (2010).

13. Ihmels H., Otto D. (2005) Intercalation of organic dye molecules into double-stranded DNA general principles and recent developments. In Wurthner F. (ed.) Supermolecular Dye Chemistry, **258**, 161-204.

14. Finichiu P.G., James A.M., Larsen L. et al. (2013) Mitochondrial accumulation of a lipophilic cation conjugated to an ionisable group depends on membrane potential, pH gradient and pK(a): implications for the design of mitochondrial probes and therapies. *J Bioenerg Biomembr* **45**, 165-173.

15. Kelso G.F., Porteous CM, Coulter CV et al. (2001) Selective targeting of a redox-active ubiquinone to mitochondria within cells - Antioxidant and antiapoptotic properties. *J Biol Chem* **276**, 4588-4596.

16. Chalmers S.,Caldwell S. T., Quin C. et al. (2012) Selective Uncoupling of Individual Mitochondria within a Cell Using a Mitochondria-Targeted Photoactivated Protonophore. *J Am Chem Soc* **134**, 758-761.

17. McQuaker S.J., Quinlan C.L., Caldwell S.T. et al. (2013) A Prototypical Small-Molecule Modulator Uncouples Mitochondria in Response to Endogenous Hydrogen Peroxide Production. *ChemBioChem* **14**, 993-1000.

18. Murphy, M.P. (2009) How mitochondria produce reactive oxygen species. *Biochem J* **417**, 1-13.

19. Quinlan C.L., Perevoschikova I.V., Goncalves R.L.S. et al. (2013) The Determination and Analysis of Site-Specific Rates of Mitochondrial Reactive Oxygen Species Production. In Cadenas E., Packer L. (eds.) Hydrogen Peroxide and Cell Signaling, Part A, **526**,189-217.

20. Pryde K.R., Hirst J. (2011) Superoxide Is Produced by the Reduced Flavin in Mitochondrial Complex I a single, unified mechanism that applies during both forward and reverse electron transfer. *J Biol Chem* **286**, 18056-18065.

21. Hirst, J. (2013) Mitochondrial Complex I. *Ann Rev Biochem* **82**, 551-575.

22. Lambert A.J., Brand, M.D. (2004) Superoxide production by NADH: ubiquinone oxidoreductase (complex I) depends on the pH gradient across the mitochondrial inner membrane. *Biochem J* **382**, 511-517.

23. Halliwell B. (2013) The antioxidant paradox: less paradoxical now? *Br J Clin Pharmacol* **75**, 637-644.

24. Smith R.A.J., Porteous C.M., Coulter C.V., Murphy, M.P. (1999) Selective targeting of an antioxidant to mitochondria. *Eur J Biochem* **263**, 709-716.

25. Dhanasekaran A., Kotamraju S., Karunakaran C. et al. (2005) Mitochondria superoxide dismutase mimetic inhibits peroxide-induced oxidative damage and apoptosis: Role of mitochondrial superoxide. *Free Radic Biol Med* **39**, 567-583.

26. Trnka J., Blaikie F.H., Smith R.A.J., Murphy, M.P. (2008). A mitochondria-targeted nitroxide is reduced to its hydroxylamine by ubiquinol in mitochondria. *Free Radic Biol Med* **44**, 1406-1419.

27. Dikalova, A.E., Bikineyeva A.T., Budzyn K. et al. (2010) Therapeutic Targeting of Mitochondrial Superoxide in Hypertension. *Circ Res* **107**, 106-116.

28. Dessolin J., Schuler M., Quinart A. et al. (2002) Selective targeting of synthetic antioxidants to mitochondria: towards a mitochondrial medicine for neurodegenerative diseases? *Eur J Pharmacol* **447**, 155-161.

29. James A.M., Sharpley M.S., Manas A.R. et al. (2007) Interaction of the mitochondria-targeted antioxidant MitoQ with phospholipid bilayers and ubiquinone oxidoreductases. *J Biol Chem* **282**, 14708-14718.

30. Kelso G.F., Maroz A., Cochemé, H.M. et al. (2012) A Mitochondria-Targeted Macrocyclic Mn(II) Superoxide Dismutase Mimetic. *Chem Biol* **19**, 1237-1246.

31. Filipovska A., Kelso G.F., Brown S.E. et al. (2005) Synthesis and characterization of a triphenylphosphonium-conjugated peroxidase mimetic - Insights into the interaction of ebselen with mitochondria. *J Biol Chem* **280**, 24113-24126.

32. Prime T.A., Blaikie F.H., Evans C. et al. (2009) A mitochondria-targeted S-nitrosothiol modulates respiration, nitrosates thiols, and protects against ischemia-reperfusion injury. *Proc Natl Acad Sci USA* **106**, 10764-10769.

33. Chouchani E.T., Methner C., Nadtochiy S.M. et al. (2013) Cardioprotection by S-nitrosation of a cysteine switch on mitochondrial complex I. *Nat Med* **19**, 753-759.

34. Quin C., Robertson L., McQuaker S.J. et al. (2010) Caged mitochondrial uncouplers that are released in response to hydrogen peroxide. *Tetrahedron* **66**, 2384-2389.

35. Murphy M.P., Holmgren A., Larsson N.G. et al. (2011) Unraveling the Biological Roles of Reactive Oxygen Species. *Cell Metab* **13**, 361-366.

36. Murphy M.P., Echtay K.S., Blaikie F.H. et al. (2003) Superoxide activates uncoupling proteins by generating carbon-centered radicals and initiating lipid peroxidation - Studies using a mitochondria-targeted spin trap derived from alpha-phenyl-N-tert-butylnitrone. *J Biol Chem* **278**, 48534-48545.

37. Quin C., Trnka J., Hay A. et al. (2009) Synthesis of a mitochondria-targeted spin trap using a novel Parham-type cyclization. *Tetrahedron* **65**, 8154-8160.

38. Xu Y.K., Kalyanaraman B. (2007) Synthesis and ESR studies of a novel cyclic nitrone spin trap attached to a phosphonium group-a suitable trap for mitochondria-generated ROS? *Free Radical Res* **41**, 1-7.

39. Hardy M., Chalier F., Ouari O. et al. (2007) Mito-DEPMPO synthesized from a novel NH2-reactive DEPMPO spin trap: a new and improved trap for the detection of superoxide. *Chem Commun*, 1083-1085.

40. Hardy M., Rockenbauer A., Vasquez-Vivar J. et al. (2007) Detection, characterization, and decay kinetics of ROS and thiyl adducts of Mito-DEPMPO spin trap. *Chem Res Toxicol* **20**, 1053-1060.

41. Dickinson B.C., Srikun D., Chang C.J. (2010) Mitochondrial-targeted fluorescent probes for reactive oxygen species. *Curr Opin Chem Biol* **14**, 50-56.

42. Robinson K.M., Janes M.S., Pehar M. et al. Selective fluorescent imaging of superoxide in vivo using ethidium-based probes. *Proc Natl Acad Sci USA* **103**, 15038-15043 (2006).

43. Kalyanaraman B., Dranka B.P., Hardy M. et al. (2014) HPLC-based monitoring of products formed from hydroethidine-based fluorogenic probes - The ultimate approach for intra- and extracellular superoxide detection. *Biochim Biophys Acta* **1840**, 739-744.

44. Cairns A.G., Senn H.M., Murphy M.P., Hartley R.C. (2014) Expanding the palette of phenanthridinium cations. *Chemistry* **20**, 3742-3751.

45. Dickinson B.C., Lin V.S., Chang, C.J. (2013) Preparation and use of MitoPY1 for imaging hydrogen peroxide in mitochondria of live cells. *Nat Protoc* **8**, 1249-1259.

46. Dickinson B.C., Chang C.J. (2008) A targetable fluorescent probe for imaging hydrogen peroxide in the mitochondria of living cells. *J Am Chem Soc* **130**, 9638-9639.

47. Van de Bittner G.C., Bertozzi C.R., Chang C.J. (2013) Strategy for Dual-Analyte Luciferin Imaging: In Vivo Bioluminescence Detection of Hydrogen Peroxide and Caspase Activity in a Murine Model of Acute Inflammation. *J Am Chem Soc* **135**, 1783-1795.

48. Van de Bittner G.C., Dubikovskaya E.A., Bertozzi C.R., Chang C.J. (2010) In vivo imaging of hydrogen peroxide production in a murine tumor model with a chemoselective bioluminescent reporter. *Proc Natl Acad Sci USA* **107**, 21316-21321.

49. Cochemé H.M., Quin C., McQuaker S.J. et al. (2011) Measurement of H_2O_2 within Living Drosophila during Aging Using a Ratiometric Mass Spectrometry Probe Targeted to the Mitochondrial Matrix. *Cell Metab* **13**, 340-350.

50. Cochemé H.M., Logan A., Prime T.A. et al. (2012). Using the mitochondria-targeted ratiometric mass spectrometry probe MitoB to measure H_2O_2 in living Drosophila. *Nat Protoc* **7**, 946-958.

51. Sikora A., Zielonka J., Lopez M. et al. (2009) Direct oxidation of boronates by peroxynitrite: Mechanism and implications in fluorescence imaging of peroxynitrite. *Free Radical Biol Med* **47**, 1401-1407.

52. Sikora A., Zielonka J., Adamus J. et al. (2013) Reaction between Peroxynitrite and Triphenylphosphonium-Substituted Arylboronic Acid Isomers: Identification of Diagnostic Marker Products and Biological Implications. *Chem Res Toxicol* **26**, 856-867.

53. Turowski M., Yamakawa N., Meller J. et al. (2003) Deuterium isotope effects on hydrophobic interactions: The importance of dispersion interactions in the hydrophobic phase. *J Am Chem Soc* **125**, 13836-13849.

54. Eltayar N., Vandewaterbeemd H., Gryllaki M. et al. (1984) the lipophilicity of deuterium atoms - a comparison of shake-flask and hplc methods. *Int J Pharm* **19**, 271-281.

55. Tanaka N., Thornton E.R. (1976) Isotope-effects in hydrophobic binding measured by high-pressure liquid-chromatography. *J Am Chem Soc* **98**, 1617-1619.

56. Logan A., Cochemé H.M., Pun P.B. L. et al. (2014) Using exomarkers to assess mitochondrial reactive species in vivo. *Biochim Biophys Acta* **1840**, 923-930.

57. Pun P.B.L., Logan A., Darley-Usmar, V. et al. (2014) A mitochondria-targeted mass spectrometry probe to detect glyoxals: implications for diabetes. *Free Radic Biol Med* **67**, 437-450.

58. Dawson M.I., Hobbs P.D. Kuhlmann K. et al. (1980) Retinoic acid analogs - synthesis and potential as cancer chemopreventive agents. *J Med Chem* **23**, 1013-1022.

59. Skulachev VP, Anisimov VN, Antonenko YN et al. (2009) An attempt to prevent senescence: a mitochondrial approach. *Biochim. Biophys. Acta* **1787**, 437-461.

Figure 1: Example bioactives targeted to the mitochondria by TPP

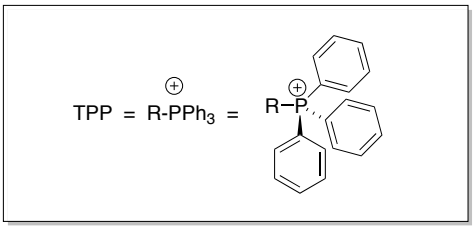

(a) Potential antioxidant drugs that react directly with ROS (some require in situ reduction to produce the active drug)

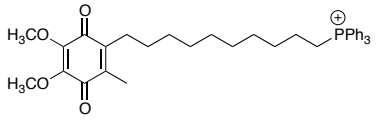

MitoQ$_{10}$ (ref 72)

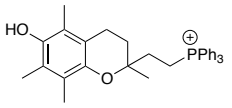

MitoE$_2$ (ref 24)

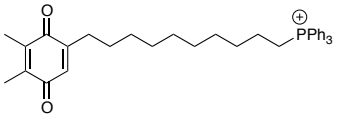

SkQ1 (ref 59)

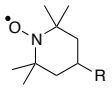

R = O(CH$_2$)$_4$PPh$_3$ **TEMPOL-TPP** (ref 28)
R = O(CH$_2$)$_5$PPh$_3$ **MitoTEMPOL** (ref 26)
R = NHCOCH$_2$PPh$_3$ **MitoTEMPO** (ref 27)

(b) Potential antioxidant drugs that catalyse the destruction of ROS

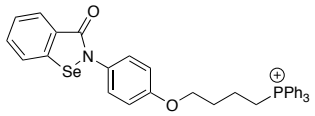

MitoPeroxidase (ref 31)

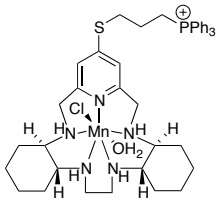

MItoSOD (30)

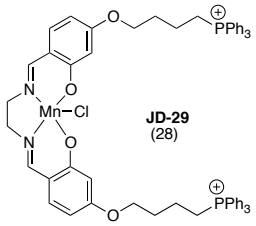

JD-29 (28)

(c) Potential antioxidant drug that affects the production of ROS

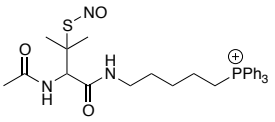

MitoSNO (ref 32)

(d) Potential antioxidant prodrug to affect ROS production in response to ROS

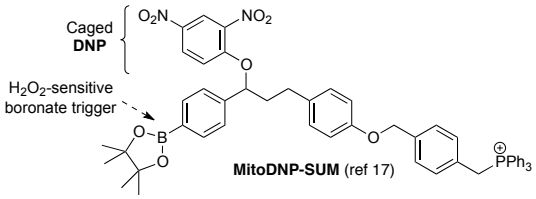

MitoDNP-SUM (ref 17)

(e) Potential prodrug that depolarises mitochondrial inner membrane in response to UV light

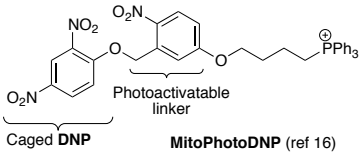

MitoPhotoDNP (ref 16)

Figure 2: The accumulation of lipophilic cation conjugates in the mitochondrial matrix due to the plasma membrane potential and the greater membrane potential across the mitochondrial inner membrane.

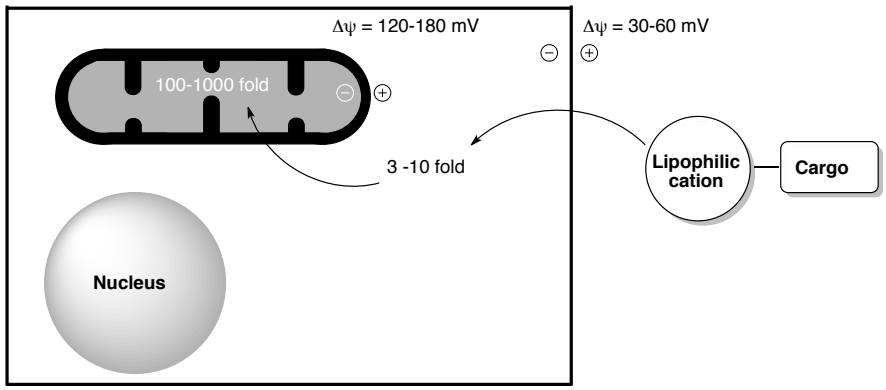

From the Nernst equation

$$\Delta\psi \text{ (in mV)} \approx 60\log_{10}\left(\frac{[\text{cation}_{in}]}{[\text{cation}_{out}]}\right)$$

@ 25 - 37 °C

10 fold accumulation for every 60 mV

Figure 3 Mechanism of accumulation of a zwitterionic TPP-carboxylate conjugate in the mitochondrial matrix.

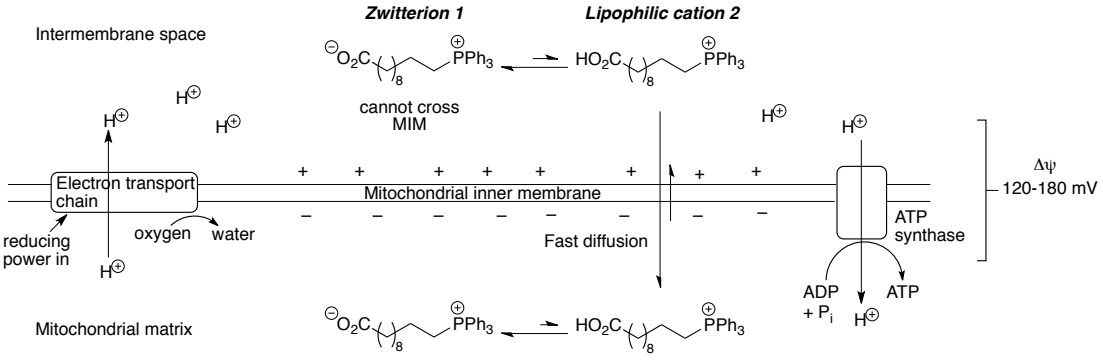

Figure 4: TPP-drug conjugates that (a) act directly as drugs, (b) are prodrugs that release the drugs in response to an instruction from outside the mitochondria, and (c) are prodrugs that release the drugs in response to an instruction from within the mitochondria.

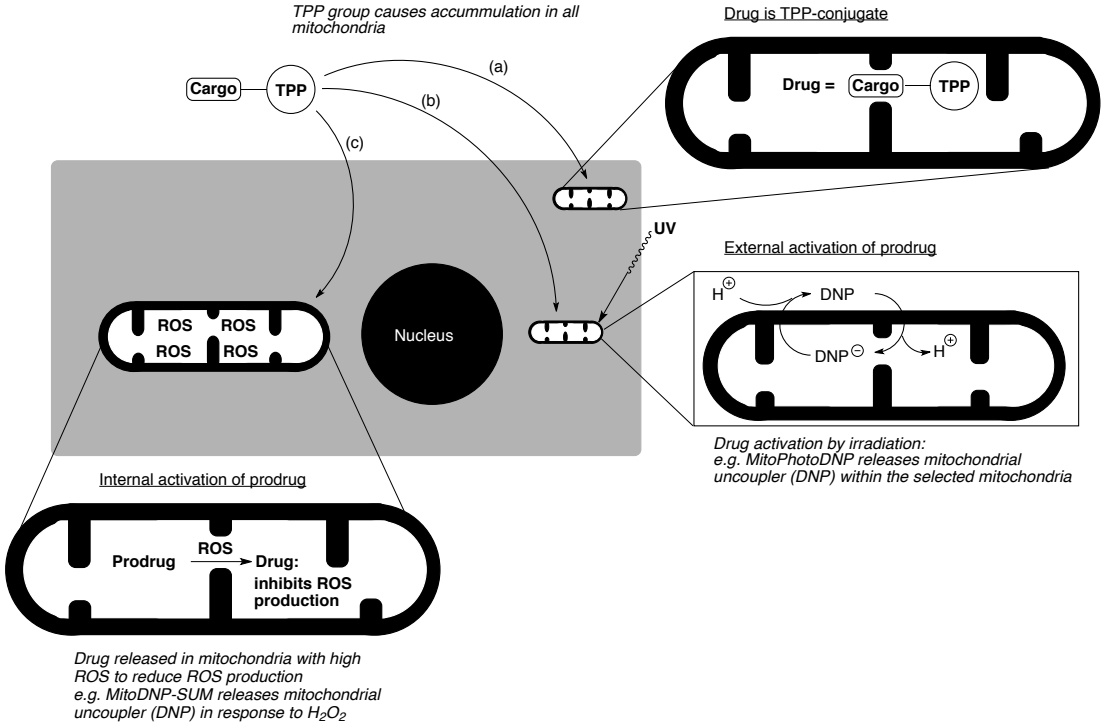

Figure 5 ROS and their generation in mitochondria

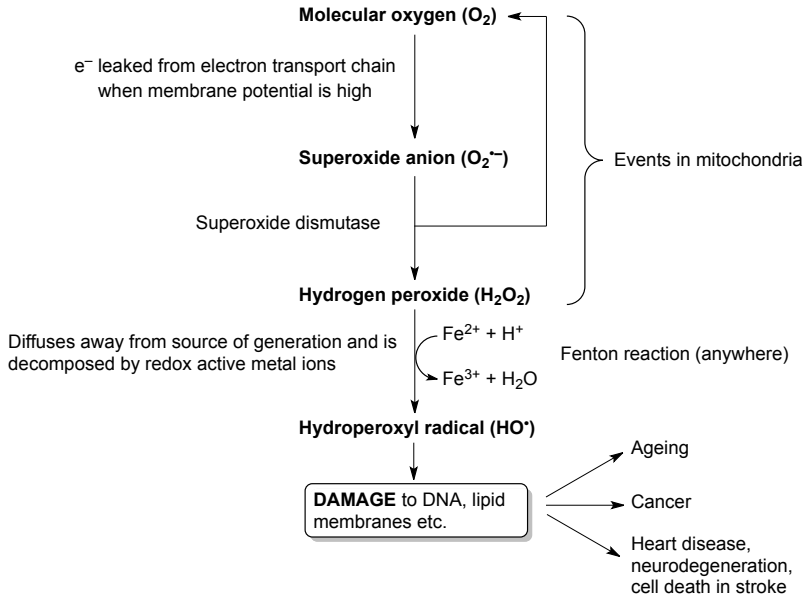

Figure 6 Release of a mitochondrial uncoupler from the mitochondria-targeted prodrug, **MitoDNP-SUM**

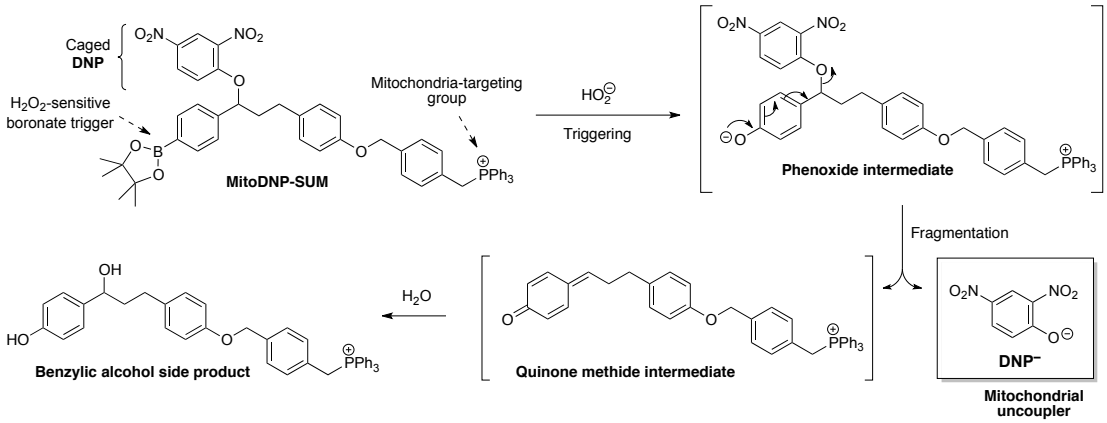

Figure 7: Examples of mitochondria-targeted sensors for detecting ROS and the products of oxidation within mitochondria

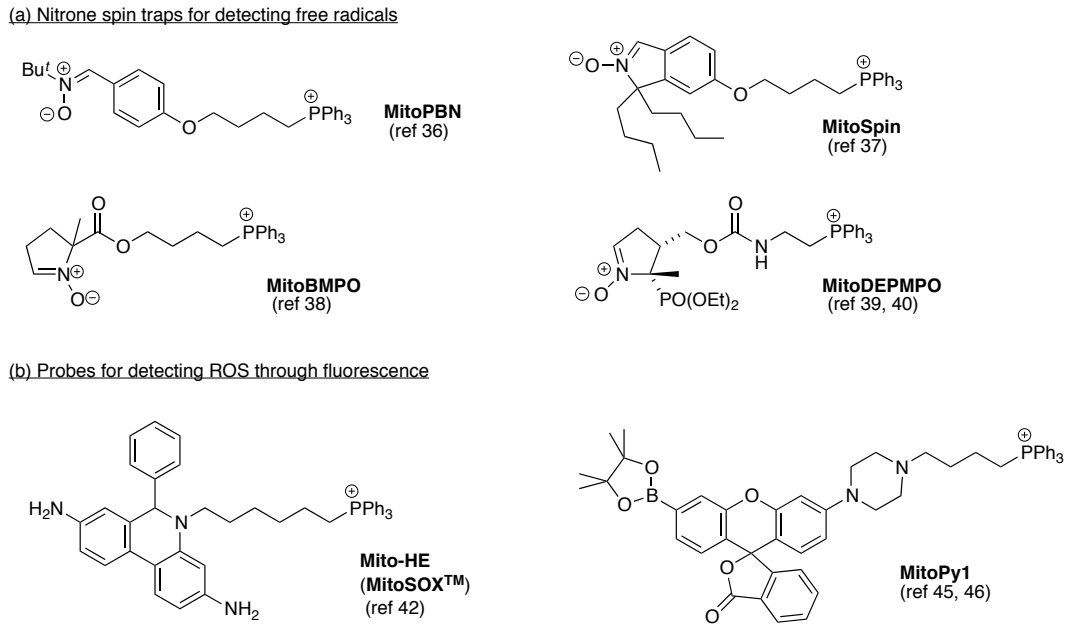

Figure 8 Reaction of **MitoB** to produce **MitoP**

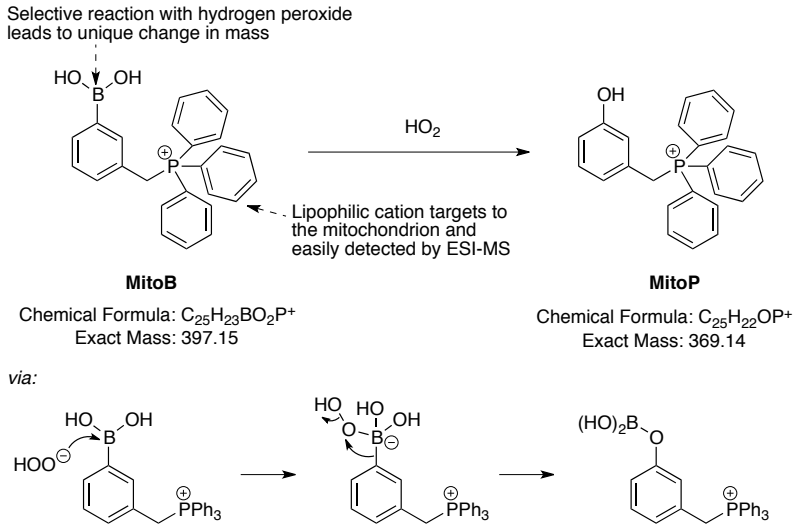

Figure 9: The molecular probe, MitoB, is converted into the exomarker, MitoP, by reaction with hydrogen peroxide inside the mitochondria, because its concentration within these organelles is approximately 3000 times the extracellular concentration and because the matrix pH is about 0.8 pH units more alkali than the cytosol. The ratio of MitoP/MitoB after a fixed period reflects the intramitochondrial [H_2O_2].

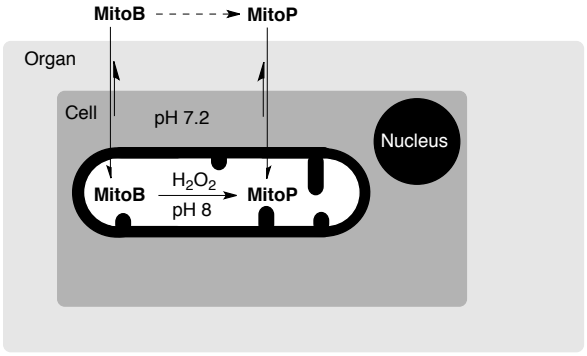

Figure 10: Synthesis of **MitoB** bromide

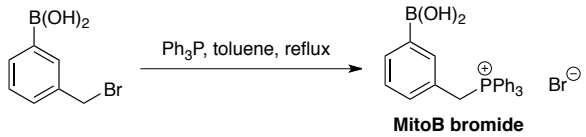

MitoB bromide

Figure 11: Synthesis of **MitoB** bromide